Catalytic Deconstruction of Ethylene Vinyl Acetate Copolymer and Polyethylene Mixtures via Hydroconversion: Challenges and Solutions

Pedro Moura[1,2], Pavel A. Kots[2], Brandon C. Vance[2], Zoé O. G. Schyns[2], Sean Najmi[2], Zachary R. Hinton[2], Caitlin M. Quinn[4], Thomas H. Epps, III[1,2,3], LaShanda T.J. Korley[1,2,3], Dionisios G. Vlachos[1,2*]

[1]Department of Chemical and Biomolecular Engineering, University of Delaware, 150 Academy St., Newark, DE 19716, USA

[2]Center for Plastics Innovation, University of Delaware, 221 Academy St., Newark, DE 19716, USA

[3]Department of Materials Science and Engineering, 127 The Green, University of Delaware, Newark, DE, 19716, USA

[4]Department of Chemistry and Biochemistry, University of Delaware, Newark, DE, 19716, USA

* Corresponding author: vlachos@udel.edu

Abstract

We explore hydrogenolysis over ruthenium supported on zirconia (Ru/ZrO_2) and hydrocracking over platinum (Pt) supported on zeolites as an effective end-of-life strategy for ethylene vinyl acetate (EVA)—a widely used performance heat-sealant in hard-to-recycle multilayer packaging. For Ru/ZrO_2 hydrogenolysis, EVA reacts slower than low-density polyethylene (LDPE), and the catalyst deactivates due to carbonaceous deposits originating from polyenes generated in situ during EVA thermal degradation. High H_2 pressures and temperatures can overcome catalyst deactivation; however, CH_4 yields are excessive due to cascade hydrogenolysis stemming from strong C=C/metal interactions. Polyene hydrogenation allows chains anchored by C=C to desorb from Ru, shifting product selectivity from CH_4 to higher-value liquids. Hydrogenolysis of mixed EVA and linear low-density polyethylene (LLDPE), mirroring typical frozen food packaging formulations, results in comparable catalyst activity and CH_4 yield as the pure EVA resin. For Pt/zeolite hydrocracking, pure EVA and EVA:LLDPE mixtures are

deconstructed to propane or light naphtha with minimal CH_4 production. Among catalysts tested, Pt/HY gives the highest liquid productivity ($g_{C5+\ products}/g_{cat}\cdot hr$). These findings showcase the recalcitrant nature of EVA and its associated mixtures for Ru/ZrO_2 hydrogenolysis, highlighting that hydrocracking catalysts may be superior for complex packaging waste.

KEYWORDS: plastics waste, valorization, hydrogenolysis, hydrocracking, ruthenium, platinum

Introduction

The overreliance of society on plastics has led to an unsustainable accumulation of plastics waste (PW). Over 8 billion metric tons of plastics have been produced to date, and over 60% of these materials have been discarded into landfills or the environment.[1] This mismanagement of waste has led to plastic leakage into the oceans, and ocean plastics are projected to overcome the weight of fish by 2050,[2] threatening both ecosystems and human health.[3] Thus, developing and implementing strategies to boost PW's recycling rates is imperative to reduce landfilling and pollution.

Mechanical recycling is a low-cost, large-scale, and low-energy approach to plastics valorization.[4] Despite its advantages, mechanical reprocessing is often challenged by mixed or multilayer PW and generates undesirable blends with poor mechanical properties[4] that are ultimately disposed of in landfills. Chemical methods, such as hydrogenolysis and hydrocracking (termed together as hydroconversion), could potentially handle such complex feedstocks. These methods are under intense development for polyolefin (PO) conversion, including low-[5–7] and high-density polyethylene (LDPE, HDPE),[7,8] linear LDPE (LLDPE), and polypropylene (PP).[6,9] Hydroconversion yields valuable hydrocarbon products, such as jet fuels and lubricants, and operates at lower temperatures than pyrolysis, which typically results in lower-value gas products.[10]

Packaging accounts for almost half of all PW,[1] and at least 10% of packaging comprises more than one polymer.[11] This compositional heterogeneity is designed to satisfy stringent packaging application requirements that cannot be met by a single polymer. For instance, packaging used in food, medical, and pharmaceutical industries, has specific technical and manufacturing requirements, such as oxygen impermeability, puncture resistance, and low-temperature sealing.[12]

Ethylene vinyl acetate (EVA), also referred to as poly(ethylene-*co*-vinyl acetate), is a specialty copolymer of ethylene and vinyl acetate (VA) primarily used in packaging due to EVA's excellent heat-sealing performance.[12] Packaging films containing 30-95% EVA are used for processed meats, frozen food, and syringes.[13] Beyond the packaging industry, EVA is also used in wire and cable insulation, photovoltaic films, and footwear soles.[14] The widespread global consumption of EVA (3.9 MMT/yr[15]) and its incorporation in hard-to-recycle films make EVA a likely component of environmentally discarded PW that is implicated in the generation of microplastics. Consequently, EVA has been reported to be present in microplastics across the world, with some containing up to 60% EVA.[16,17] To the best of our knowledge, there have been no studies on the hydroconversion of EVA or the impact of EVA on PE hydrogenolysis with specific relevance to PE-EVA films.

Herein, we showcase EVA's conversion over ruthenium supported on zirconia (Ru/ZrO_2), a common PO hydrogenolysis catalyst.[18,19] By modulating the starting resin and reaction conditions, we explore the effect of vinyl acetate content, H_2 pressure, and temperature on the final EVA deconstruction chemistry. We then expand our study to examine the deconstruction of EVA:LLDPE mixtures representing films containing EVA, such as films used in frozen food packaging. We demonstrate that hydrogenolysis of EVA and EVA:LLDPE mixtures under typical operating conditions (250 ºC, 30 bar H_2) performs poorly, producing elevated yields of low-value CH_4. Importantly, we introduce hydrocracking catalysts that achieve conversions comparable to

Ru/ZrO_2, generating high-value liquid products and overcoming undesirable CH_4 yields in hydrogenolysis.

Results and Discussion

EVA Hydrogenolysis and Solid Residue Characterization

We chose EVA resins of 12 and 40 wt% vinyl acetate (EVA-12 and EVA-40, respectively) for initial hydrogenolysis experiments to span across most common EVA applications,[14] such as multilayer films and fabric coatings. These reaction results were benchmarked against those from LDPE hydrogenolysis in single feedstock experiments. The Ru/ZrO_2 catalyst is made up of ~2.5 nm Ru-metal clusters (Fig. S1a-c) dispersed on mesoporous (Table S1) ZrO_2 nanoparticles (Fig. S1d). In 1.5 h, Ru/ZrO_2 catalyzed hydrogenolysis converts 79 wt% of LDPE and yields 38 wt% gaseous (C1-C6) and 39 wt% soluble products (C7-C35) (Fig. 1a). Methane yield is 27 wt% and comprises most of the gaseous product (72%), with the remainder being C2-C6 (Fig. 1b). The liquid products span mainly C7-C17 (Fig. 1c) with diesel yields (C9-C22) at 29 wt%, comprising 74% of liquid products; lubricant base oil range products (C20-C50) are obtained at 10 wt% yield. The catalyst structure, activity, and selectivity are all comparable with prior literature.[18] In contrast to LDPE, Ru/ZrO_2 converts only 41 wt% of EVA-12 (vs. 79% conversion for LDPE) primarily to CH_4 (Fig. 1a-c). Similarly, the catalyst activity for EVA-40 is even lower (30 wt% vs. 41 wt% conversion for EVA-12), with CH_4 as the exclusive hydrocarbon product, and 6 wt% H_2O (not shown) as the sole liquid (Fig. 1a-c). Extending reaction times (for EVA-12) does not yield liquid products and leads to catalyst deactivation (Fig. 1d). Changing the Ru catalyst support to CeO_2 leads to similar results as with ZrO_2—specifically, solid and CH_4 yields increase ~3x and ~2x, respectively, when comparing LDPE to EVA-12 hydrogenolysis (Fig. S2). Overall, these findings expose EVA's recalcitrant nature to hydrogenolysis.

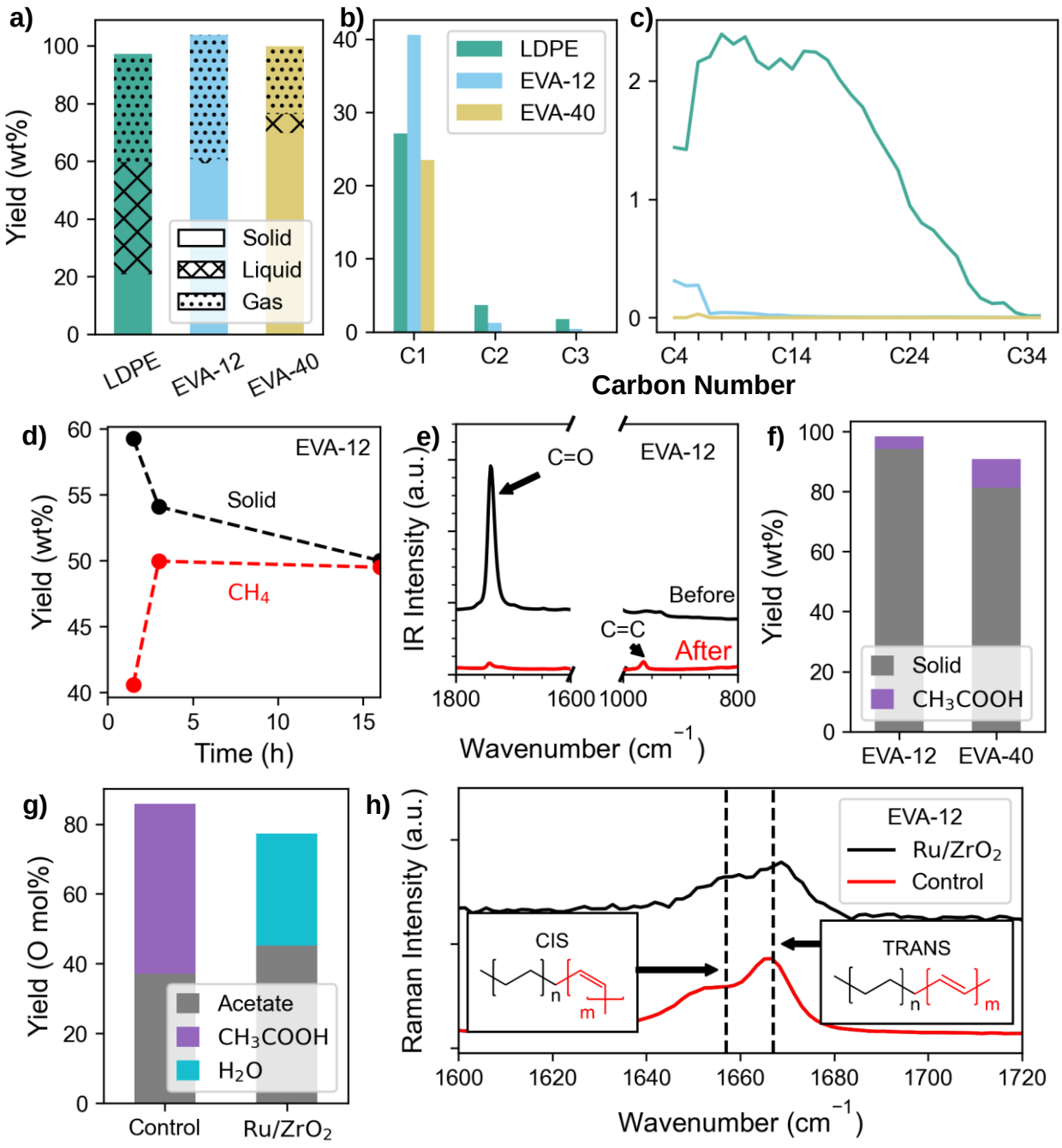

Figure 1. Hydrogenolysis of EVA resins and solid residue analysis. (a-c) Overall and detailed hydrogenolysis product yields from LDPE and EVA resins. (d) Time-dependent hydrogenolysis of EVA-12. (e) ATR-FTIR spectra of EVA-12 solids before and after hydrogenolysis. (f) Product yields of control experiment (thermal decomposition) without a catalyst. (g) Oxygen balance in EVA-12 hydrogenolysis over Ru/ZrO_2 and in control experiment. (h) Raman spectra of solid residues after

EVA-12 hydrogenolysis and control. Reaction conditions: 250 ºC, 30 bar H_2, 1.5 h, 2 g substrate, 0.05 g Ru/ZrO_2. The total mass yield for the second data point in Fig. 1d at t=3 h is above 100 wt% by <5 wt% due to the experimental error associated with CH_4 quantification.

Spectroscopic analysis of solid residues by attenuated total reflectance-Fourier infrared (ATR-FTIR) spectroscopy reveals that the v(C=O) peak at 1740 cm^{-1}, corresponding to the acetate pendent group of pristine EVA, is reduced after hydrogenolysis (Fig. 1e). However, a new peak forms at 964 cm^{-1} indicating the presence of trans v(C=C)[20] moieties (Fig. 1e, Fig. S3a). Raman and ^{13}C solid-state nuclear magnetic resonance (SS NMR) spectroscopy corroborate the formation of C=C moieties (Fig. S3b-e) characteristic of vinyl polymers [*i.e.*, poly(vinyl chloride), poly(vinyl acetate), or poly(vinyl alcohol)][21] undergoing thermal degradation to form polyenes.[20] Notably, EVA follows an acetate thermal decomposition mechanism, forming acetic acid (CH_3COOH) and C=C after thermal degradation of a six-member ring transition state made by hydrogen bonding between the acetate pendant group and the adjacent methylene group (Scheme 1).[22] It is known that this degradation mechanism can lead to crosslinking,[23] which is supported by oscillatory rheological measurements (frequency sweeps) of the solid residues, in which the storage modulus (G' > G'') dominates across the whole frequency range;[24,25] Fig. S4. Consequently, it is likely that crosslinking during hydrogenolysis lowers the H_2 availability[26] in the polymer melt by increasing the melt viscosity[27] causing olefin moieties to remain after hydrogenolysis (*i.e.*, lack of C=C hydrogenation); further discussed in the SI.

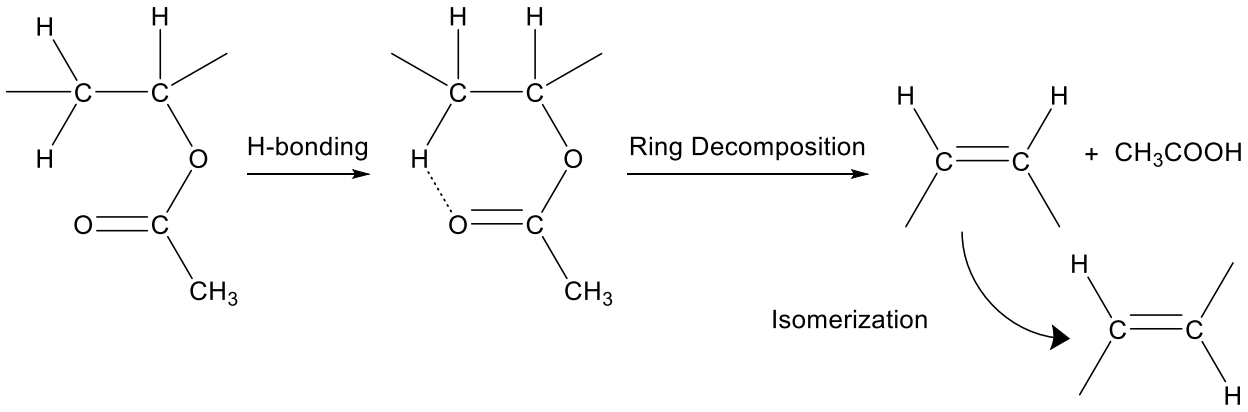

Scheme 1. EVA acetate pendent group thermal decomposition mechanism via six-member ring transition state.[22]

A control experiment of thermal decomposition of EVA without a catalyst shows that EVA is moderately converted (<20 wt% conversion) to a mixture of solid and CH_3COOH (Fig. 1f). According to a total oxygen balance, thermal degradation converts 49% of EVA's acetate groups to CH_3COOH (Fig. 1g, Control), and Raman spectra of the solid residue display a shoulder at 1657 cm^{-1} and a peak at 1667 cm^{-1} corresponding to cis and trans ν(C=C), respectively (Fig. 1h).[28] The presence of C=C resembles the hydrogenolysis solid (Fig. 1h, Fig. S5) and indicates that unsaturated carbon backbones originate from EVA's thermal degradation. In contrast to the control experiment, CH_3COOH is not obtained after hydrogenolysis as 32% of EVA's acetate groups are converted exclusively to H_2O (Fig. 1g, Ru/ZrO_2). Prior work on CH_3COOH hydrogenation on Ru (at similar temperatures of 225 ºC) demonstrated high conversion of CH_3COOH to CH_4, CO, and CO_2 (Scheme 2, R1&2).[29,30] However, neither CO nor CO_2 were detected in our gas products after hydrogenolysis [according to gas chromatography-thermal conductivity detector (GC-TCD)], indicating that intermediate CO/CO_2 converts to CH_4 and H_2O (Scheme 2, R3&4). In summary, CH_3COOH generated from EVA's thermal degradation, or its intermediates, undergoes complete hydrodeoxygenation (HDO) to H_2O and CH_4 (Scheme 2, R5),

and CH_3COOH may compete with EVA for Ru sites, inhibiting EVA hydrogenolysis.

$$CH_3COOH + H_2 \longrightarrow CH_4 + CO + H_2O \quad (R1)$$

$$CH_3COOH \longrightarrow CH_4 + CO_2 \quad (R2)$$

$$CO+3H_2 \longrightarrow CH_4 + H_2O \quad (R3)$$

$$CO_2+4H_2 \longrightarrow CH_4 + 2H_2O \quad (R4)$$

$$CH_3COOH + 4H_2 \longrightarrow 2CH_4 + 2H_2O \quad (R5)$$

Scheme 2. Reaction sequence for CH_3COOH hydrodeoxygenation over Ru metal.

Our analysis above suggests that *in-situ* polyene and/or CH_3COOH formation [Fig. 1(f,h)] deactivates the Ru/ZrO_2 catalyst. This hypothesis is supported by thermogravimetric analysis-mass spectrometry (TGA-MS) of EVA-12 residues (Fig. S6), revealing temperature-induced evolution of coke precursors (benzene, toluene, and xylene), consistent with prior literature.[31] Furthermore, carboxylic acids are notorious for dissolving and oxidizing metals, including Ru,[32] which can alter the catalyst structure or reduce the number of metallic sites for hydrogenolysis, leading to deactivation. To elucidate the catalyst deactivation, we assessed each species' role in hydrogenolysis.

Identification of Catalyst Deactivating Species

Initially, we added the quantity of CH_3COOH that would theoretically be generated by eliminating all acetate groups in EVA-12—twice the quantity lost in the hydrogenolysis experiment—to LDPE and probed its effect on the final deconstruction. Adding CH_3COOH (160 µL) slowed the overall reaction rate at 1.5 h, resulting in an increase of solid yield from 38 wt% to 80 wt% and dropped the liquid yield from 39 wt% to 3 wt% (Fig. 2a). Methane is generated as the dominant product at slightly lower yields (22 wt% vs. 27 wt% for LDPE without CH_3COOH) (Fig. 2b) along with a relatively flat carbon distribution for larger hydrocarbons <0.2 wt% (Fig. 2c).

Despite LDPE hydrogenolysis being retarded by CH_3COOH, the reaction still proceeds at the longer reaction times of 3 h [Fig. 2(a-c)]. At 3 h, the solid yield decreases to 32 wt% and the liquid yield increases to 22 wt% (Fig. 2a) with a CH_4 yield of 33 wt% (Fig. 2b)—remarkably, solid yields remain higher than LDPE without CH_3COOH (32 wt% vs. 20 wt%) even though the reaction is twice as long. CH_3COOH is absent according to gas chromatography-mass spectrometry (GC-MS), and we attribute the increased methane yield (27 wt% for LDPE 1.5 h vs. 33 wt% in LDPE+CH_3COOH 3 h) in part to 1) CH_3COOH undergoing complete HDO to H_2O and CH_4 (Scheme 2, R5) (maximum estimated as ~4 wt% CH_4), and 2) LDPE C-C scission from terminal carbons. Furthermore, the liquid products are centered at heavier hydrocarbons, around C22 (Fig. 2c), suggesting that CH_3COOH impacts hydrogenolysis beyond affecting the rate of backbone C-C scission. Even though the loss of acetate groups is thought to occur directly on the Ru catalyst via intermediates rather than forming CH_3COOH per se, these experiments demonstrate that CH_3COOH and its intermediates could slow the reaction kinetics. Yet, CH_3COOH does not appear to permanently prevent the C-C backbone scission and is likely not responsible for catalyst deactivation in EVA hydrogenolysis. Results herein suggest that the acid retards the cracking of the polymer chain due to strong competitive adsorption compared to polyethylene chains.

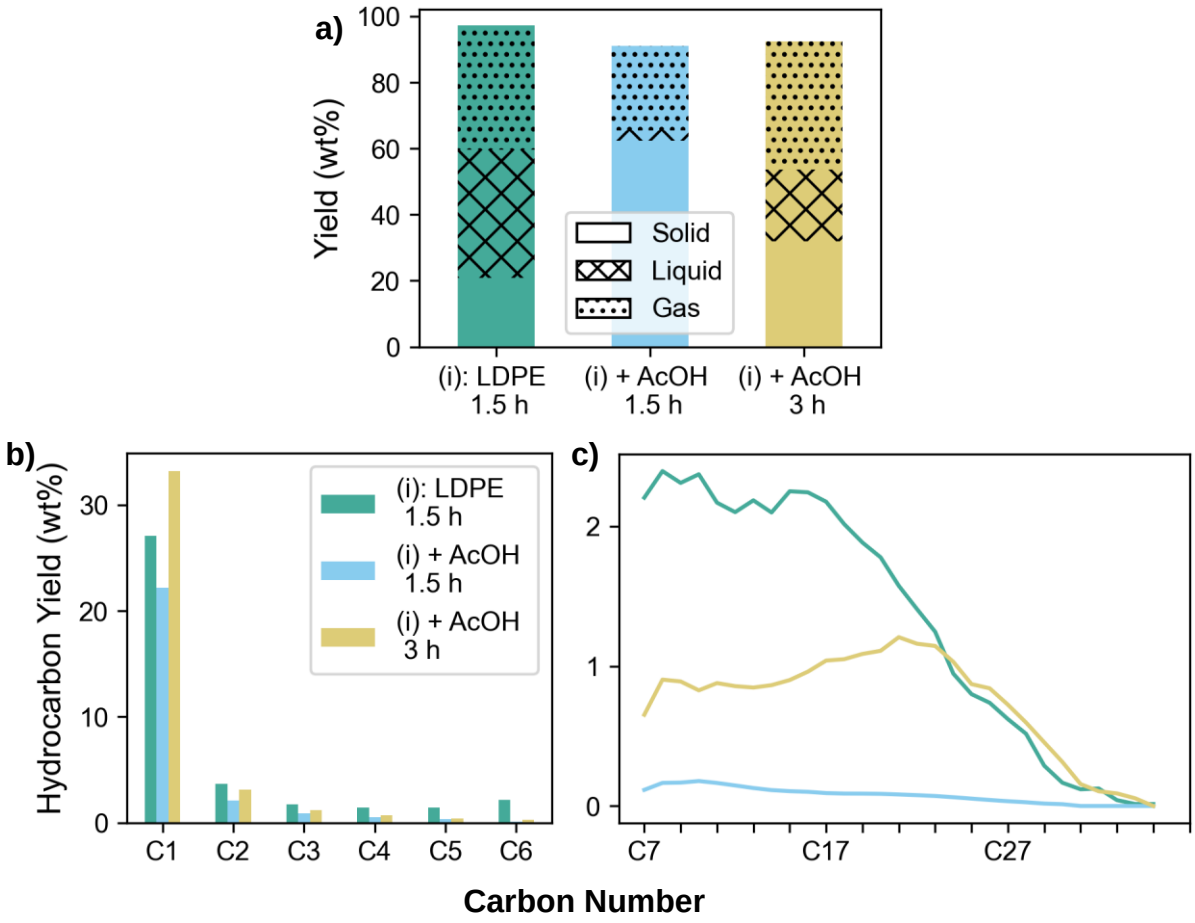

Figure 2. Effect of CH_3COOH on LDPE deconstruction. (a-c) Overall and detailed product yields in LDPE hydrogenolysis as a reference and when CH_3COOH has been added. Reaction conditions: 250 ºC, 30 bar, 0.05 g Ru/ZrO_2, 2 g LDPE, reaction time as indicated. No oxygenated products were detected in GC-MS.

We further analyzed the polyenic residues from EVA hydrogenolysis and the control experiment by differential scanning calorimetry (DSC). Pristine EVA-12 DSC traces reveal a melting peak at 93 ºC (Fig. 3a, Pristine) corresponding to ethylene domains and an overall 28% crystallinity (calculated relative to the melting enthalpy for 100% crystalline PE,[33] Equation 4 - Methods). The solid from the control experiment has a melting point and crystallinity of 98 ºC and 30%, respectively (Fig. 3a, Control), due to the loss of bulky acetate pendent groups that disrupt

crystalline regions formed by ethylene domains. Thus, we assign this DSC peak (Fig. 3a, Control) to the melting point of the solid residue containing polyene segments. The melting point and the crystallinity of the solid after EVA hydrogenolysis over Ru/ZrO_2 increase to 101 ºC and 34% (Fig. 3a, Ru/ZrO_2), respectively. Hydrogenolysis of the polymer chains is expected to generate subpopulations of smaller chains, leading to the broadening of DSC features into lower-temperature regions.[18] Instead, our results show a single melting peak, suggesting that the solid residue containing polyene segments is highly recalcitrant and is not broken down into small chains by hydrogenolysis.

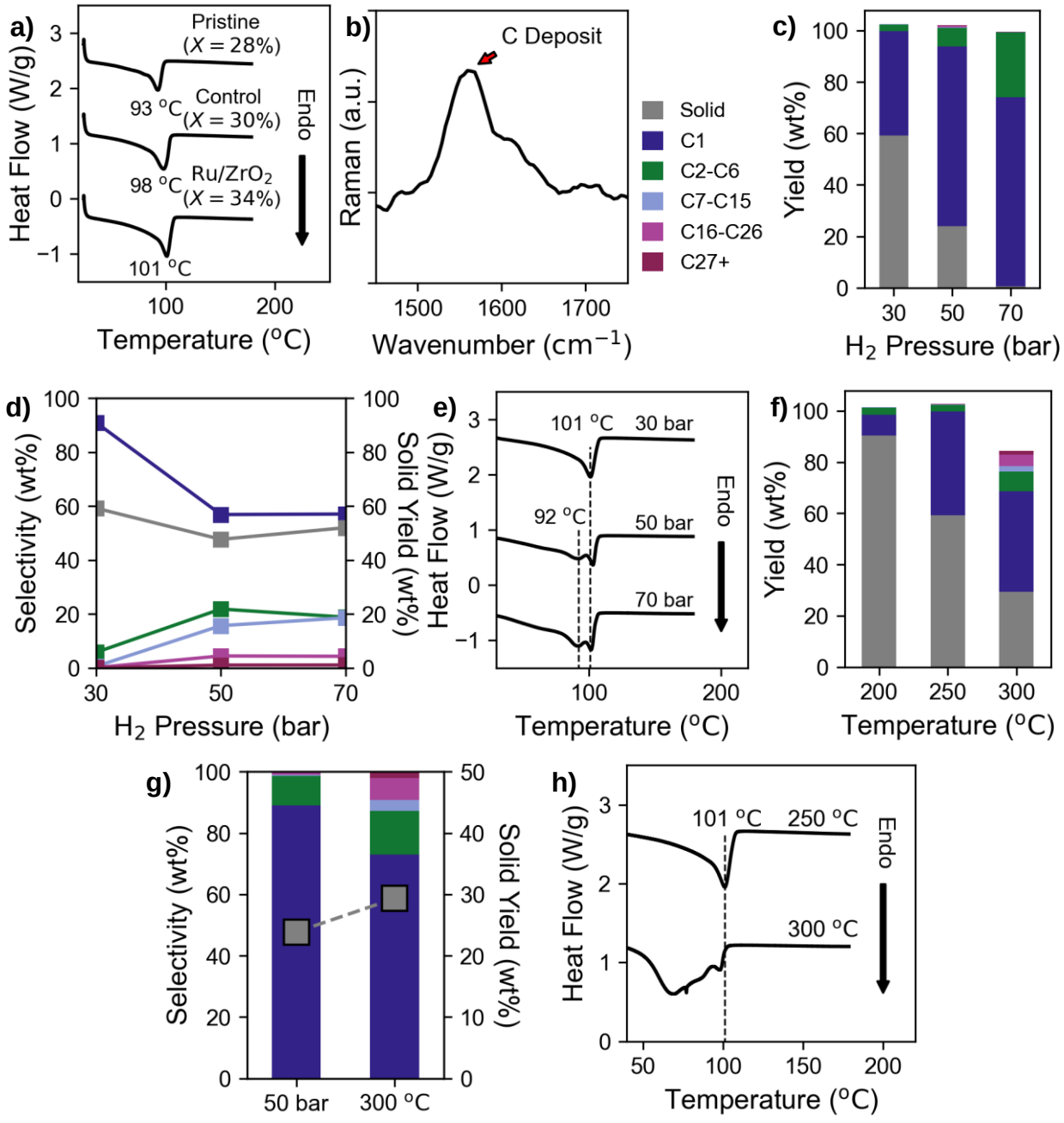

Figure 3. H_2 and temperature effect for EVA-12 over Ru/ZrO_2 and solid residue analysis. (a) DSC of pristine EVA-12 and solids after hydrogenolysis (Ru/ZrO_2) and without a catalyst (Control). (b) Raman spectroscopy of spent catalyst after EVA-12 hydrogenolysis. (c) Product yields for EVA-12 hydrogenolysis at different H_2 pressures. (d) Product selectivities at similar solid conversions (1.5 h for 30 bar and 0.75 h for 50 and 70 bar) and (e) respective DSC of solid products. (f) Product yields for EVA-12 hydrogenolysis at different temperatures. (g) Product

selectivity and solid conversions at 50 bar and 300 ºC. (h) DSC of solid samples for (f). Reaction conditions: 250 ºC, 2 g EVA-12, 30 bar, 1.5 h, 0.05 g Ru/ZrO_2 (unless stated otherwise). Dashed lines (e,f) indicate melting points in the solid samples.

The Raman spectrum of the spent catalyst (Fig. 3b) shows a peak at 1560 cm^{-1} corresponding to pairs of unsaturated sp^2 carbon[34] and derivative thermogravimetry (DTG) shows two small peaks at 325 and 490 ºC (Fig. S7), corresponding to soft and hard coke, respectively.[35] Both results indicate that carbonaceous deposits on the catalyst's surface form during EVA hydrogenolysis— a reasonable finding considering coke precursors are found in the TGA-MS of the polymer residue (Fig. S6). These carbonaceous deposits most likely block Ru active sites and prevent cracking of unreacted chains (Fig. 3a), leading to deactivation (Fig. 1d). The catalyst activity is recovered upon adding fresh catalyst to the polyenic residue, after which 73 wt% of the residue is converted exclusively to CH_4 (Fig. S8). Overall, our study of the solid residues and the spent catalyst provides strong evidence that carbon deposits from polyenes formed during EVA thermal degradation are responsible for the deactivation of Ru/ZrO_2, aligning with prior pyrolytic studies.[36] We attempted to test this hypothesis by adding 1-octadecene as a polyene probe molecule to LDPE hydrogenolysis. No significant deactivation occurred (*i.e.*, within 10% conversion, Fig. S9), most likely due to the viscosity difference between the olefin and the EVA melt (~7 orders of magnitude, Fig. S10), rendering the olefin incapable of adequately probing the deactivation mechanism by polyenes in the EVA melt (see further discussion in the SI).

Altogether, our results suggest that EVA will interfere with PE hydrogenolysis, reducing process efficiency and output value. To test this hypothesis, we mixed EVA with LLDPE to emulate frozen food packaging compositions (30% EVA and 70% LLDPE). Similar outcomes were found in comparison to pure EVA, with a slightly higher conversion of 56 wt% (vs. 41 wt%), a high CH_4

yield of 43 wt%, and 11 wt% C2-C6 (Fig. S11), further corroborating the inability of Ru/ZrO_2 to generate high-value liquid products from EVA-containing plastic feedstocks.

Parametric Studies and Insights

To tackle the recalcitrant polyene, we increased the H_2 pressure to enhance the hydrogenation of the C=C bonds and the hydrogenolysis rate in the C-C backbone. As shown in Fig. 3c, increasing the H_2 pressure from 30 to 50 bar H_2 more than doubles the amount of EVA converted (~60% vs. 25% solid yield). Methane remains the dominant product at 70 wt% yield, with C2 as a side product at 6 wt%. We achieve complete conversion of EVA at 70 bar H_2 with product yields of 73 wt% to CH_4 and 21 wt% C2. Although these findings demonstrate that increasing pressure can overcome catalyst deactivation, the high yields of CH_4 generated render the deconstruction of EVA over Ru/ZrO_2 unappealing from an environmental/industrial perspective.

A comparison of our EVA hydrogenolysis results and those in the literature for PO hydrogenolysis reveals intriguing similarities and differences. First, the hydrogenolysis rate of C-C backbones of both feedstocks exhibits a positive order with respect to H_2 pressure[18](Fig. 3c), indicating low hydrogen coverage on the Ru sites. Second, under similar EVA conversions, our findings show that increasing H_2 pressure up to 70 bar decreases the product selectivity of CH_4 by 33% (Fig. 3d) and boosts selectivity to longer alkyl products, specifically C2-C6 and liquid C7-C15 products to ~16% each. This H_2-promoted suppression of CH_4 and consequential increase of longer alkyl products has been reported for LDPE hydrogenolysis and is characteristic of a cascade hydrogenolysis mechanism proposed by Wang et al.[18] Notably, Wang et al. demonstrate that for LDPE hydrogenolysis, increasing H_2 pressures from 50 to 130 bar (at 250 ºC) resulted in carbon product distributions shifting to higher alkanes (C15+) due to increased hydrogenation and desorption of cleaved C-C backbones on Ru. In contrast to PO, the selectivity benefit of increased H_2 pressure to heavy products does not extend past C15 products for EVA hydrogenolysis (Fig. 3d). ATR-FTIR and DSC traces of the solid residues confirm the presence of a trans ν(C=C) peak

at 964 cm^{-1} (Fig. S12) and of a melting peak at ~101 ºC (Fig. 3e), respectively, indicating the presence of polyene segments after hydrogenolysis at 50 and 70 bar. According to the cascade hydrogenolysis mechanism, high yields of CH_4 and low selectivity to longer alkanes, like those reported here for EVA, are symptomatic of chains that crack extensively due to their slow desorption from the Ru surface.[18] We hypothesize that polyene segments from thermally degraded EVA chains, even under highly reducing atmospheres (Fig. S12), over-bind onto Ru,[37] desorb slowly, and crack by cascade bond scissions leading to CH_4[18] (Scheme 3).

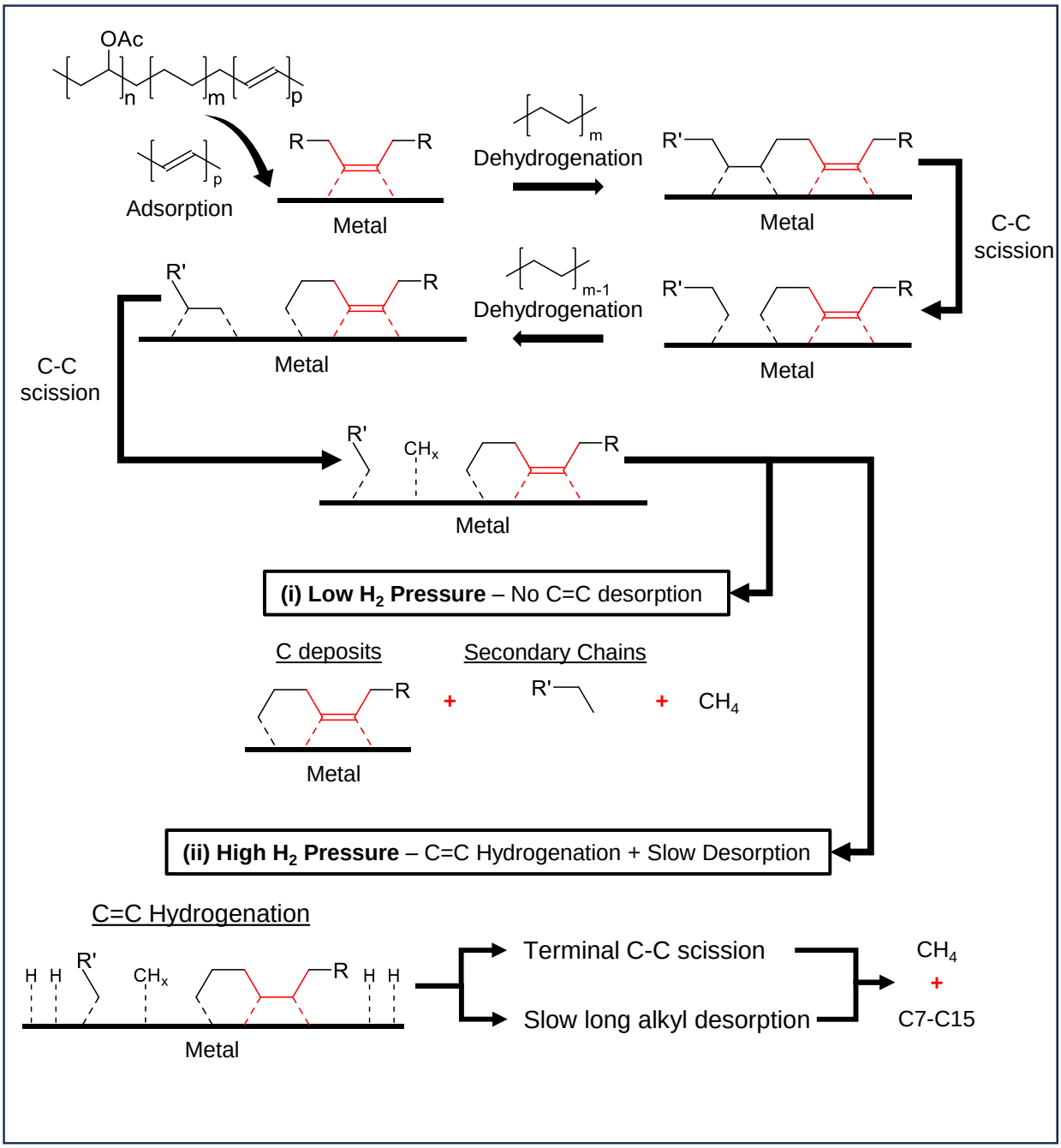

Scheme 3. Proposed mechanism for adsorption of polyene segments on Ru/ZrO_2 and product formation at low (i) and high (ii) H_2 pressures. R = $[CH_2CH(CH_3COO)]_n$-$[CH_2CH_2]_m$-$[CHCH]_{p-1}$; R' = $[CH_2CH(CH_3COO)]_n$-$[CH_2CH_2]_{m-1}$-$[CHCH]_{p-1}$]

At low H_2 pressures (30 bar), VA repeat units, which are isolated between ethylene segments and constitute over 88% of the VA population in EVA-12,[38] thermally degrade into polyene segments that anchor on Ru sites, leading to cascade backbone cracking occurring predominantly on adjacent ethylene segments (Scheme 3i). Furthermore, DSC analysis after hydrogenolysis at 30 bar shows that the crystallinity of the solid residue increases to 34% [vs. 30% for the control experiment (Fig. 3a)]. ^{13}C SS NMR corroborates this observation (Fig. S13), for which the ratio between peaks at ~33 and 31 ppm corresponding to crystalline and amorphous CH_2 segments, respectively,[39] is higher after hydrogenolysis than in the uncatalyzed control experiment (1.3 vs. 1.1). These findings suggest that leftover VA repeat units react with Ru once chains adsorb on the metal surface, resulting in the additional loss of acetate pendant groups. This loss of VA coupled with decreases in molecular weight facilitates crystallization of the sample,[39] as evidenced by increases in crystallinity calculated from DSC analyses. Size exclusion chromatography (SEC) of the solid residue displays a bimodal distribution (Fig. 4a) with two distinct populations centered at 10^3 and ~10^4 (g/mol), and further analysis by SEC-infrared (SEC-IR) reveals that these populations have distinctly different concentrations of VA repeat units (Fig. 4b). This contrast in VA concentration and molar mass distribution between the two chain populations reveals a disparity in hydrogenolysis rates for each chain population. Specifically, shorter chain populations (centered at ~10^3 g/mol) underwent extensive hydrogenolysis compared to longer chain populations (centered at ~10^4 g/mol) and have a significantly lower concentration of VA (at least two-fold), supporting the prior hypothesis that VA segments react with Ru once chains are adsorbed. We postulate that this bimodal distribution and disparity of VA concentrations is due to catalyst particles being non-uniformly distributed throughout the polymer melt during the reaction. Therefore, we propose that two distinct regions exist in the melt; the first is a catalyst-poor region in which deconstruction is dominated by uncatalyzed thermal degradation, resulting in higher molecular weights and VA concentrations (*i.e.*, the overlapping populations centered at ~10^4 g/mol in Fig. 4a for Control and Ru/ZrO_2). The second is a catalyst-rich region in which

deconstruction is dominated by Ru/ZrO_2-catalyzed hydrogenolysis, resulting in lower molecular weights and VA concentrations (*i.e.*, the population centered at ~10^3 g/mol in Fig. 4a, Ru/ZrO_2).

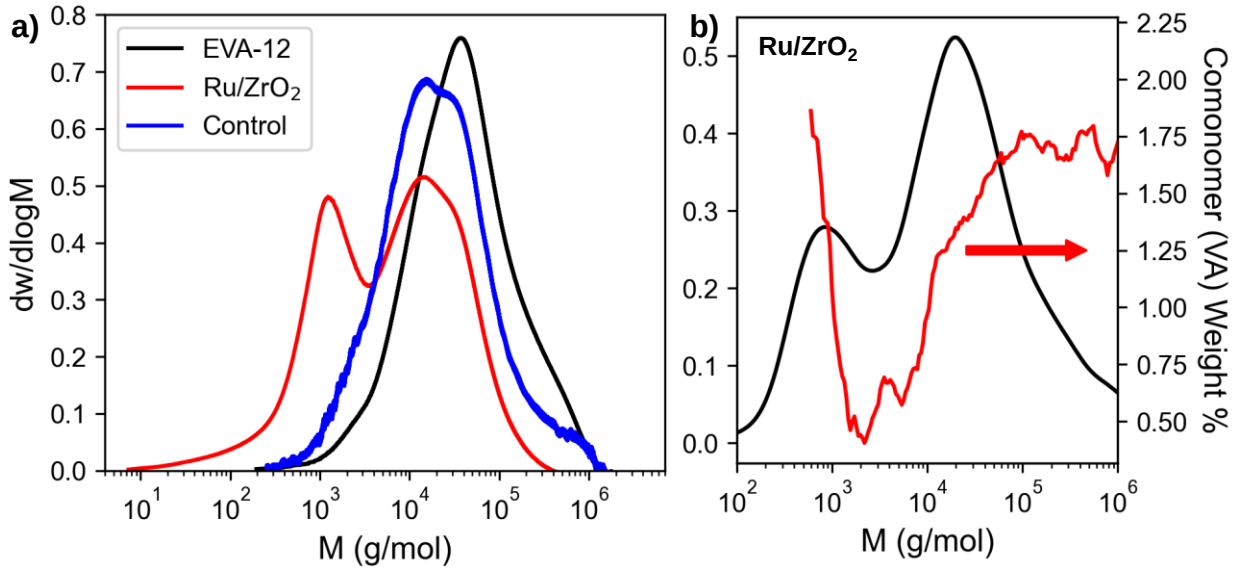

Figure 4. SEC and SEC-IR analysis of EVA-12 and solid products after reaction with and without Ru/ZrO_2. (a) Molecular mass distribution of EVA-12, solid products after EVA-12 hydrogenolysis over Ru/ZrO_2, and after control experiment (without catalyst). (b) Molecular mass distribution and VA wt% of corresponding distribution of solid products after EVA-12 hydrogenolysis over Ru/ZrO_2.

At high H_2 pressures (50/70 bar), the DSC melting peak at 101 ºC of the polyenic solid residue is smaller in comparison to the polyenic solid residue formed from low H_2 pressure reaction (30 bar), and a new feature appears in the DSC trace at 92 ºC (Fig. 3e), which is attributed to hydrogenation of C=C and C-C scission of chains, generating saturated chains of lower molecular weight. Notably, the trans ν(C=C) peaks at 964 cm^{-1} in ATR-FTIR spectra have lower peak intensities (Fig. S12), *i.e.*, the polyene generated in situ adsorbs on the Ru surface and is

hydrogenated either 1) fully, resulting in saturated chains desorbing, or 2) partially, followed by cracking to CH_4 or longer alkyl products (Scheme 3ii).

Next, we studied the effect of temperature on EVA hydrogenolysis. As shown in Fig. 3f, low quantities of solid are converted at 200 ºC (<10 wt%), combined with a balance of CH_4 (8 wt% yield) and C2-C6 (3 wt% yield). The reaction at 300 ºC results in 71 wt% conversion with product yields of 39 wt% CH_4, 8 wt% C2-C6, and 8 wt% C7+. Interestingly, increasing the temperature enhances product selectivity to liquid alkanes (C7+) more than increasing H_2 pressure (Fig. 3g) (13 wt% vs. 1 wt%, respectively) and lowers CH_4 selectivity, a result that differs from PO hydrogenolysis.[5] DSC analysis of residues from experiments at 300 ºC indicates that the melting peak at 101 ºC of the solid residue is almost completely absent; instead, a broad melting range centered around 68 ºC appears, indicating a distribution of molecular weights and chain structures (Fig. 3h). Additionally, ATR-FTIR spectra do not show the presence of C=C bonds in the solid residue (Fig. S14).Together, these results indicate that polyene segments generated *in-situ* are hydrogenated on Ru, and then undergo further cracking into shorter chains followed by desorption from the surface (Scheme 3ii). Our analysis suggests that *in-situ* saturation of polyenes is a vital strategy to achieve greater selectivity to heavier hydrocarbons in the hydrogenolysis of EVA. Hence, the development of catalyst alternatives should prioritize catalysts that can saturate C=C, such as those used in the hydrogenation of polybutadienes,[40] and retain significant activity for hydrogenolysis.

Hydrocracking of EVA and PE Mixtures

For EVA conversion, one can exploit the in situ formation of C=C to create another core strategy to alleviate the catalyst activity, product selectivity, and catalyst stability challenges related to Ru/ZrO_2. Specifically, hydrocracking catalysts use a bifunctional mechanism in which metal sites produce olefins that crack on acid sites and migrate back to metal sites to be hydrogenated and produce alkanes.[41] According to this cracking mechanism, we hypothesize that

polyene segments generated *in-situ* by thermal degradation will crack further on acid sites. Furthermore, hydrocracking catalysts containing an active hydrogenation component may be more robust and less selective to CH_4 than hydrogenolysis catalysts. To investigate this hypothesis, we tested a platinum-supported HY (Pt/HY) hydrocracking catalyst for the deconstruction of EVA. This choice was based on two main considerations. First, Pt is recognized to display increased activity for hydrogenation in comparison to Ru,[42] and should partially reduce the degree of unsaturation of polyene segments and increase hydrogenation rates for the products of acid site-catalyzed cracking. Second, HY contains strong acid sites capable of cracking C=C bonds through a carbocation mechanism.[8] Promisingly, when switching to Pt/HY-catalyzed EVA deconstruction, the CH_4 yield is greatly reduced in comparison to Ru/ZrO_2-catalyzed deconstruction (1 wt% vs. 41 wt% yield, respectively) at similar conversions (60 wt% solid yield) (Fig. 5a) and mainly C4-C6 products (19 wt% total yield) are obtained (Fig. 5b). Time-course experiments indicate that a maximum yield of ~51 wt% >C2 products is obtained by extending the reaction time up to 6 h (Fig. S15). These C4-C6 products are more desirable than CH_4 as they are widely used as feedstocks in the petrochemical industry.[43]

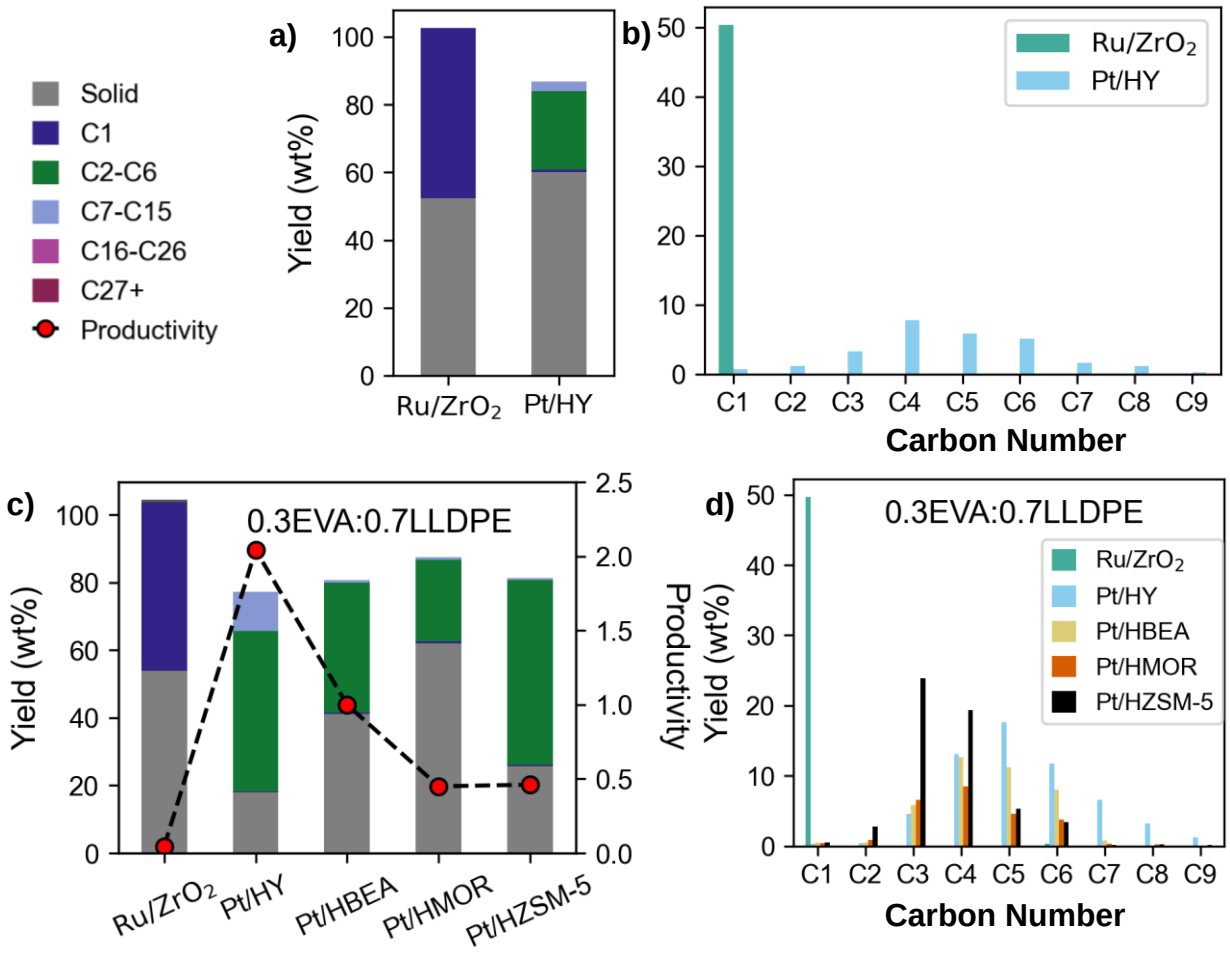

Figure 5. EVA-12 and PE mixture deconstruction over Pt-zeolites. Overall (a) and detailed (b) hydroconversion product yields from EVA-12 resins over Ru/ZrO_2 and Pt/HY catalysts. Overall (c) and detailed (d) hydroconversion product yields from a mixture of 30% EVA-12 and 70% LLDPE over Ru/ZrO_2 and various Pt-containing zeolites. Reaction conditions: 250 ºC, 30 bar, 2 h, 2 g substrate, and polymer:catalyst mass ratio = 10:1.

Given the capability of Pt/HY to produce higher-value products, we explored additional zeolites (*i.e.*, HBEA, HMOR, HZSM-5) for the hydrocracking of a mixture of EVA and LLDPE (chosen as a mixture representative of packaging films). Almost all catalysts resulted in higher conversion of EVA/LLDPE mixtures into more valuable products (no CH_4) in comparison to

Ru/ZrO_2 (Fig. 5c-d). Pt/HY converts 82 wt% of the mixture to mostly C4-C6 at 43 wt% total yield, respectively, with C3, C7, and C8 as side products. In contrast to Pt/HY, Pt/HBEA-catalyzed hydrocracking does not yield products larger than C6. Quantification of zeolite acid densities by Pyridine-IR reveals that Pt/HBEA has a higher concentration of Brønsted acid sites compared to Pt/HY (344 and 233 μmol/g, respectively; Table S1). Our findings are in qualitative agreement with work completed by Liu et al.[8] demonstrating that zeolite Brønsted acid densities are positively correlated with shorter alkane product selectivity. PtHZSM-5 produces lighter C3 and C4 products at 24 and 19 wt% yields, respectively, whereas Pt/HY-catalyzed reaction yields C4 and light naphtha (C5-C6). We postulate that this product difference is due to the smaller pores of Pt/HZSM-5 compared to Pt/HY—as evidenced by the lack of mesopores >5 nm (Fig. S16) and a smaller mesoporous surface area (78 vs. 262 m^2/g; Table S1)—denying pore entry to EVA-polyenic chains, causing them to initially crack on external acid sites before allowing smaller fragments to diffuse inside small pores and crack further. Of the catalysts tested, Pt/HY gave the highest liquid productivity, defined as $g_{C5+\ products}/g_{cat}\cdot h$, making it a promising catalyst for upcycling PO films containing EVA (Fig 5c). Furthermore, despite carbonaceous deposits forming on the spent Pt/HY catalyst after reaction (~1.8 wt% soft and ~5.8% hard coke; Fig. S17), the catalyst performance is reasonably maintained after regeneration by calcination in static air (580 ºC, 4 h) following reduction treatment (250 ºC, 2 h in 50% H_2 flow; Fig. S18). Specifically, the heavier products increase due to a minor loss in activity (*i.e.*, <10% EVA conversion), which we attribute to the decrease in Pt dispersion (Table S2). Overall, these results suggest that hydrocracking catalysts are better suited for converting mixtures of EVA and POs of real packaging waste films than common hydrogenolysis catalysts, such as Ru/ZrO_2.

Conclusions

In this article, we investigated the hydrogenolysis of EVA and EVA/LLDPE mixtures on Ru/ZrO_2, a typical hydrogenolysis catalyst. Pure EVA-12 resin demonstrated lower conversions

relative to LDPE and this rate decrease was exacerbated by increasing vinyl acetate content of EVA (EVA-40). Deconstruction of EVA-12 and LLDPE mixtures (emulating frozen food packaging) via hydrogenolysis leads to similar catalytic activities as pure EVA, with CH_4 as the dominant product across all reactions involving EVA. Acetate groups in both EVA-12 and EVA-40 thermally degrade into CH_3COOH and polyene segments. Although CH_3COOH was found to retard C-C scission in LDPE hydrogenolysis (by outcompeting LDPE for Ru sites and undergoing HDO to H_2O and CH_4), *post-mortem* analysis of spent catalysts revealed that recalcitrant polyene segments in the residue were responsible for catalyst deactivation. Catalyst deactivation was overcome by hydrogenation of polyene segments at increased H_2 pressures, although at the expense of high CH_4 yields. These high amounts of CH_4 are rationalized by a cascade mechanism featuring strong anchoring and slow desorption of polyenic chains. Similar to PO hydrogenolysis, H_2 pressure accelerates the deconstruction rate and suppresses CH_4 formation. High temperatures are unexpectedly more selective to liquids due to *in-situ* hydrogenation of polyene segments. In contrast to hydrogenolysis over Ru/ZrO_2, Pt/zeolite hydrocracking catalysts overcame the major catalyst deactivation and dominant CH_4 formation by leveraging carbocation chemistry; the polyene segments formed thermally are cracked on acid sites and diffuse to the metal sites to be hydrogenated and desorb. Specifically, all Pt/zeolite catalysts crack EVA and EVA:LLDPE mixtures with comparable conversion to Ru/ZrO_2-catalyzed cracking (±~20%) with minimal CH_4 production (<1% yield), and high yields of C3-C6 products. Moreover, Pt/HY was found as the most productive catalyst for liquid products of all tested with 2.04 $g_{C5+\ products}/g_{cat}\cdot h$. Overall, our results suggest that the direct application of hydroconversion catalysts may not be effective in generating high-value alkanes from multilayer films. Yet, the learnings presented herein can be leveraged to develop high-performance catalysts that are well suited to valorize ubiquitous packaging waste streams.

Experimental Section

Catalyst Synthesis

Catalysts were synthesized by wet impregnation method. ZrO_2 was synthesized by calcining $ZrO_x(OH)_{4-2x}$ for 4 h at 550 ºC (2 ºC/min). $ZrO_x(OH)_{4-2x}$ was made according to prior literature.[18] HY(30) [*i.e.*, HUSY(30)], ZSM-5(23), MOR(20), and BEA(25) were bought from Zeolyst International with the SiO_2/Al_2O_3 mole ratio indicated in parenthesis. All supports, including CeO_2 (Alfa Aesar, 044960.22), were calcined prior to impregnation for 4 h at 550 ºC (2 ºC/min). Ruthenium(III) nitrosyl nitrate ($Ru(NO)(NO_3)_x(OH)_{3-x}$, Aldrich, 1.5 wt% Ru) and Chloroplatinic acid (8 wt% in H_2O, Aldrich) precursors were measured based on metal amounts corresponding to theoretical metal loadings of 5 and 0.5 wt% on Ru and Pt catalysts, respectively. After impregnation, the slurries were dried at 110 ºC overnight with 0.5Pt/Zeolites being calcined again. All catalysts were then reduced in a tubular reactor at 250 ºC under 100 sccm He flow with 10% H_2 for ruthenium and 50% H_2 for platinum catalysts. Nominal metal weight loadings were consistent across Ru and Pt catalysts, and their values of 5 and 0.5 wt% are omitted in the text.

Catalyst Characterization

Bright-field transmission electron microscopy (BF-TEM) was performed with a field emission gun transmission electron microscope (JEOL, JEM-2010F), operated at an accelerating voltage of 200 kV. Catalyst samples were diluted in acetone and deposited on a lacey carbon film on copper grids (Electron Microscopy Sciences). Metal loadings and zeolites SiO_2:Al_2O_3 ratios were confirmed by elemental analysis using a wavelength-dispersive X-ray fluorescence (WDXRF, Rigaku, Supermini 200) spectrometer equipped with a high-powered (200 W) X-ray tube. The BET surface area and porosity were measured using N_2 as the adsorbent at 77 K with a Micromeritics ASAP 2020 instrument. H_2 temperature programmed reduction (H_2-TPR) of Ru/ZrO_2 was performed on an AutoChem II 2920 (Micromeritics) installed with a TCD detector; 0.1 g of catalyst was first annealed under He (50 mL/min) at 200 ºC for 1 h and then cooled to 60 ºC, followed by heating to 900 ºC (10 ºC/min) in a flow of 10 vol % H_2/Ar (50 mL/min). The H_2-TPR

scan (Fig. S19) indicates that Ru/ZrO_2 is completely reduced to a metallic state after reduction treatment. CO pulse chemisorption was performed in the same AutoChem to measure Pt dispersion at 30 ºC in 10% CO/Ar (30 mL/min); 0.1 g samples were reduced in 30 mL/min 10%H_2/Helium flow (400 ºC, 2 h, 2 ºC/min) prior to CO chemisorption (Table S2). X-ray diffraction (XRD) crystallography was performed on Ru/ZrO_2 and ZrO_2 using a Bruker D8 diffractometer equipped with a Cu K_α source; Ru crystalline patterns are absent in the Ru/ZrO_2 catalyst (Fig. S20) due to the small Ru particle size (< 5nm) according to TEM (Fig. S1).

Acid site density measurements were performed using FTIR transmission spectra of pyridine and recorded in a homemade Pyrex flow cell equipped with KBr windows. Catalyst samples were pressed in a self-supported wafer and placed in a cell sample holder. Before measurements, the sample was reduced in the flow cell (30 mL/min) for 2 h at 250 °C in 50% H_2/He flow. Then, the sample temperature was lowered to 150 °C and followed by a ~5 µL injection of pyridine (99.8%; Sigma-Aldrich) in He flow. After injection, the sample was flushed with He until no changes in the spectra were observed. Then, the temperature was increased with at 10 °C/min to 350 °C in a flow of He, and spectra were recorded every 15 °C. Peak integration was performed using OMNIC software; calculation of Brønsted and Lewis acid site densities was done according to prior methods.[44] Values for catalyst characterization properties and TEM images of Ru particles on ZrO_2 are in the supplementary information (Table S1, Fig. S1).

Catalytic Experiments

LDPE [~72 kDa weight-average molecular weight (M_w)], LLDPE (~127 kDa M_w), EVA-12 (~92 kDa M_w), and EVA-40 (~59 kDa M_w) resins were purchased from Sigma Aldrich. Representative molecular weight distributions measured by SEC are given in Fig. S21. Reactions were performed in a 50-mL Parr reactor and charged with a predetermined amount of catalyst and resin. All catalysts were freshly reduced and used within 24 h before reaction. The headspace was purged 5x with H_2 before charging to the designated reaction pressure. Afterward, the reactor was heated

to reaction temperature using a band heater, and stirring was initiated at 500 rpm with a polytetrafluoroethylene (PTFE) magnetic stirrer bar upon reaching 10 ºC above the highest melting point of the substrate. Reactions were terminated by quenching the autoclave in an ice bath.

Water content in the products was determined using a Mettler Toledo V20 Karl Fischer volumetric titrator. Composite-5 in anhydrous methanol (Hydranal) was used as the titrant. Less than 1 mL of the sample was weighed and injected into the mixing chamber pre-filled with Hydranal.

For product quantification of the hydroconversion reactions, gaseous products were collected with a Tedlar bag at 5 ºC and analyzed using an Agilent 8890A GC-FID equipped with an Agilent HP-Plot GC column. Standard calibration mixtures were used to quantify gaseous hydrocarbon products. Deconstruction products from PE were extracted from the reactor using ~20 mL of dichloromethane (CH_2Cl_2, Fisher Scientific, ACS grade), whereas those from EVA were extracted with tetrahydrofuran (HPLC Grade, Fisher Chemical) to allow for H_2O quantification. 20 mg of n-octacosane (TCI chemicals,>98%) was added to extraction solvents as an external standard. Quantification of n-C_{28} products was estimated by averaging the FID signal between n-C_{27} and n-C_{29}. The soluble products were analyzed using GC-MS (Agilent, HP-5ms column) for identification and GC-FID (Agilent HP-1 column) for quantification. A representative raw GC trace is shown in Fig. S22. Standard calibration mixtures using n-alkanes were used for liquid hydrocarbon quantification, with response factors assumed to be the same for isomerized alkanes. The catalyst and remaining solids were filtered, dried in air overnight, and weighed prior to further characterization.

The following equations were used to calculate the mass yield of products (Y_i)

$$Y_i = \frac{m_{i,product}}{m_{resin}} \times 100\% \quad (1)$$

with $m_{i,product}$ as the mass of each extracted product; m_{resin} is the measured mass of polymer used prior to a reaction. Overall mass balances are calculated as $M.B. = \Sigma Y_i$, which were at the lowest 77% (Fig. 5c, Pt/HY). Product selectivity (S_i) was calculated as:

$$S_i = \frac{Y_i}{\Sigma Y_{i,non-solid}} \times 100\% \quad (2)$$

with $Y_{i,non-solid}$ as the combined mass yields of liquid and gas products (Table S4). Oxygen balances were calculated on a molar basis:

$$O.B. = \frac{\Sigma n_O, product}{\Sigma n_O, initial} \times 100\% \quad (3)$$

with initial moles of oxygen ($n_O, initial$) quantified by TGA of EVA resins; moles of oxygen in products ($n_O, product$), specifically acetate groups in solids, H_2O, and CH_3COOH [GC-MS also detected negligible amounts (<0.5 wt%) of ethyl acetate, acetone, ethanol, and acetaldehyde in the control experiment (Fig. 1f)] are quantified by ATR-FTIR spectroscopy, Karl Fisher Titration, and GC-FID, respectively. Ru/ZrO_2 samples in Fig. 1g were melt blended to improve the detection of the C=O ATR-FTIR signal (i.e., Fig. 1e) resulting from the non-uniform distribution of Ru/ZrO_2 particles in the sample. Control samples were not melt blended, potentially resulting in acetate underestimation. Experimental error for conversion and phase yields were below 15%.

Catalyst Regeneration

Pt/HY catalyst caked on the filter after product filtration was recovered and regenerated by calcination in a muffle furnace at 580 ºC for 4 h (2 ºC /min) followed by a reduction in a tubular reactor at 250 ºC under 100 sccm He flow with 50% H_2.

Solid Residue Characterization

DSC (Discovery TA Instruments) experiments were conducted under N_2 flow. Samples were sealed in aluminum pans and heated to 180 ºC (10 ºC/min) to remove thermal history, after which

they were cooled (5 ºC/min), followed by a second heating to 180 ºC (10 ºC/min). The second heating curve was used for analysis in the main text.

Crystallinity calculations were done relative to the melting enthalpy of 100% crystalline PE ($\Delta H^{o}_{m,100\%\ cryst.\ PE}$= 293 J/g)[33] and the equation:

$$X\ (\%\ crystallinity) = \frac{\Delta H_{m,sample}}{\Delta H^{o}_{m,100\%\ cryst.PE}} \times 100 \quad (4)$$

$\Delta H_{m,sample}$ represents the melting enthalpy of the sample calculated by DSC.

Thermogravimetric analysis (Discovery TA Instruments) experiments were conducted under N_2 flow of 80 mL/min (or Air for spent catalyst) from 250-550 ºC at 20 ºC/min. Weight losses between 300-400 ºC corresponding to CH_3COOH were multiplied by the molecular ratio between VA and CH_3COOH (1.43) to determine the amount of VA in solid samples; VA amounts in commercial EVA resins of 12, 18, and 40 wt% VA were within 2% of their nominal amounts (Table S3).

Thermogravimetric analysis-mass spectrometry was performed on a TGA5500 (TA instruments) coupled to an MKS Cirrus 3 mass spectrometer with a secondary electron multiplier. Approximately 5 mg of sample was loaded onto each pan and heated in 20 sccm of N_2 at 20 ºC/min. The samples were equilibrated at 30 ºC before ramping to 550 ºC. Detected masses ranged from 1-128 amu.

Rheological characterization was performed on a TA instruments DHR3 (20mm parallel plates) under Peltier plate heating. Samples were loaded onto pre-heated test geometries (150 ºC) before they were slowly pressed and trimmed such that the final testing thickness was 0.8–0.9 mm. Samples were left to equilibrate at temperature for 5 minutes, and a pre-shear step was applied at 0.1 1/s for 60 s to remove stresses associated with sample loading. Amplitude sweeps were performed at 150 °C, 10 rad/s, 0.1–10% strain to identify determine the oscillation strain within the linear viscoelastic region for further testing. Frequency sweeps were performed at 0.5% strain

from 0.5–500 rad/s. Cox-Merz transformations were applied to frequency sweeps to relate the complex viscosity to the shear viscosity. Zero shear viscosities were calculated by fitting the Carreau-Yasuda Model to the transformed frequency sweeps.

ATR-FTIR spectra of solid residues and pristine EVAs were measured using a Nicolet Nexus 640 spectrometer with a Smart Orbit Diamond ATR accessory in the mid-IR range (4000−650 cm^{-1}). A calibration curve for measuring unknown amounts of VA in samples was established according to the wt% of VA in EVA commercial resins as calculated by TGA and the ratio of the ν(C=O) peak in the 1740 cm^{-1} region to the ν(C-H) peak in the 1460 cm^{-1} region.[45] Prior to analysis, melt blending of Ru/ZrO_2 (1.3–3.6 g) samples was performed in a HAAKE Minilab 3 Micro Compounder. Samples were loaded under N_2 purge and melt compounded for 3 min at 180 °C and 100 rpm under N_2. Samples were extruded after 3 min and cooled at ambient temperature.

Raman spectra were measured on a Horiba LabRAM HR evolution spectrometer using a 532 nm green laser and a 325 nm He-Cd excitation UV laser.

All SS-NMR spectroscopy measurements were carried out on a Bruker AVANCE III HD spectrometer operating at a proton resonance frequency of 600.13 MHz. Samples were packed in a zirconia rotor with a Kel-F cap and spun at 14 kHz. A ^{13}C direct polarization pulse sequence was used with a 3.6 μs 90° pulse, 85 kHz proton decoupling, and a recycle delay of 30 s. For each spectrum, 256 scans were collected and averaged at room temperature.

Molecular weight characterization of solid residues (including pristine polymers) was performed via SEC using a HT-GPC TOSOH HLC-8312GPC/HT. The solid residues were dissolved in 1,2,4-trichlorobenzene at 140 ºC (hydrogenolysis residues were dissolved at 165 ºC). The clear polymer solution was decanted from the catalyst particles and reconstituted in the mobile phase [1,2,4-trichlorobenzene with 500 ppm butylated hydroxytoluene (BHT)] at 2 mg/mL concentration and heated for at least 2 h at 140 °C. 300-μL injections of sample solutions were eluted at 0.8 mL/min

at 140 °C through two TSKgel GMHHR-H(20)HT columns in series, with detection via refractive index (RI) and differential viscometer detectors. Molecular weight calculations were calibrated using nine narrow polystyrene standards and corrected according to the Mark-Houwink relationships for PE and polystyrene (following prior work[46]).

GPC/SEC-IR analytical services of solid residues were provided by Polymer Char. Analyses were performed in a HT-GPC instrument, model GPC-IR (Polymer Char, Paterna, Spain). The instrument was configured as a dual detection system consisting of an IR6 multiple band filter-based IR detector (CH channel: IR absorbance 2800–3000 cm^{-1} and CO channel centered at 1740 cm^{-1}) and a four-capillary bridge viscometer, with 3 PLgel Olexis Mix-Bed 13 µm (Agilent) for molar mass separation. The columns compartment temperature was 150 ºC, pump flow rate 1.0 mL/min and injection volume 200 µL. The mobile phase was oDCB, stabilized with 300 ppm BHT. The polymer samples were dissolved at a concentration of 1.0 mg/mL in the same solvent used as mobile phase, at 160 ºC for 1 h. Molar mass distributions and averages were obtained applying a universal calibration measured with polystyrene standards and with online determination of intrinsic viscosity with the system viscometer for the analyzed polymers. The concentration chromatogram was calculated using the IR CH absorbance with a correction for the VA content based on the CO channel. Analytical differences between SEC and SEC-IR measurements for Ru/ZrO_2 in Fig. 4 are attributed to different method conditions and the non-uniform composition of solid products.

Supporting Information: Catalyst characterization, including H_2-TPR, CO chemisorption, TEM, XRD, N_2 physisorption, XRF, and Py-IR. Resin characterization by SEC and TGA. Solid product characterization by ATR-FTIR, Raman, ^{13}C SS-NMR, and TGA-MS. Spent Pt/HY TGA and regeneration experiments. Additional Ru/ZrO_2 hydrogenolysis experiments, including over Ru/CeO_2 (PDF).

Author Contributions

P.M.: conception, experiments, analysis, writing. P.A.K. and B.C.V: conception, analysis. Z.O.G.S.: Microcompounding, SEC experiments, rheological characterization, analysis, editing. S.N. and C.M.Q.: NMR experiments and analysis. Z.R.H.: SEC experiments and analysis. T.H.E. and L.T.J.K.: advisement on SEC analysis, funding acquisition. D.G.V.: conception, editing, funding acquisition. All authors have reviewed the manuscript.

Declaration of Competing Interest

The authors declare no known competing financial interests or personal relationships that could have appeared to influence the work reported in this paper.

Acknowledgments

The bulk of this work was done by P.M. and supported under a Project Award Agreement from the National Institute for Innovation in Manufacturing Biopharmaceuticals (NIIMBL) and financial assistance award 70NANB21H085 from the U.S. Department of Commerce, National Institute of Standards and Technology. S.N. was supported by the National Science Foundation under Grant No. OIA – 2119754. Z.O.G.S. was supported as part of the Center for Plastics Innovation, an Energy Frontier Research Center funded by the U.S. Department of Energy (DOE), Office of Science, Basic Energy Sciences (BES), under award DE-SC0021166 (HT-GPC and microcompounding). We also acknowledge using instruments in the Advanced Materials Characterization Lab (AMCL). The use of NMR facilities at the University of Delaware was supported by a grant from the National Institute of General Medical Sciences – NIGMS (5 P30 GM110758-02) from the National Institutes of Health. P.M. acknowledges Christine M. Oberhausen for providing feedback on the manuscript, Jessie A. Sun for conducting the BET/BJH measurements for Ru/ZrO_2, and Esther López from Polymer Char who provided the sample analysis data by GPC-IR.

References

(1) Geyer, R.; Jambeck, J. R.; Law, K. L. Production, Use, and Fate of All Plastics Ever Made. *Science Advances* **2017**, *3* (7). https://doi.org/10.1126/sciadv.1700782

(2) World Economic Forum. *The New Plastics Economy the Future of Plastics*; 2016.

(3) Prata, J. C.; da Costa, J. P.; Lopes, I.; Duarte, A. C.; Rocha-Santos, T. Environmental Exposure to Microplastics: An Overview on Possible Human Health Effects. *Science of the Total Environment*. Elsevier B.V. February 1, 2020. https://doi.org/10.1016/j.scitotenv.2019.134455.

(4) Schyns, Z. O. G.; Shaver, M. P. Mechanical Recycling of Packaging Plastics: A Review. *Macromolecular Rapid Communications*. Wiley-VCH Verlag February 1, 2021. https://doi.org/10.1002/marc.202000415.

(5) Rorrer, J. E.; Beckham, G. T.; Román-Leshkov, Y. Conversion of Polyolefin Waste to Liquid Alkanes with Ru-Based Catalysts under Mild Conditions. *JACS Au* **2021**, *1* (1), 8–12. https://doi.org/10.1021/jacsau.0c00041.

(6) Nakaji, Y.; Tamura, M.; Miyaoka, S.; Kumagai, S.; Tanji, M.; Nakagawa, Y.; Yoshioka, T.; Tomishige, K. Low-Temperature Catalytic Upgrading of Waste Polyolefinic Plastics into Liquid Fuels and Waxes. *Appl Catal B* **2021**, *285*, 119805. https://doi.org/10.1016/j.apcatb.2020.119805.

(7) Qiu, Z.; Lin, S.; Chen, Z.; Chen, A.; Zhou, Y.; Cao, X.; Wang, Y.; Lin, B.-L. A Reusable, Impurity-Tolerant and Noble Metal-Free Catalyst for Hydrocracking of Waste Polyolefins. *Science Advances* **2023**, *9* (25). https://doi.org/10.1126/sciadv.adg5332

(8) Liu, S.; Kots, P. A.; Vance, B. C.; Danielson, A.; Vlachos, D. G. Plastic Waste to Fuels by Hydrocracking at Mild Conditions. *Science Advances* **2021**, *7*, 8283–8304. https://doi.org/10.1126/sciadv.abf8283

(9) Kots, P. A.; Liu, S.; Vance, B. C.; Wang, C.; Sheehan, J. D.; Vlachos, D. G. Polypropylene Plastic Waste Conversion to Lubricants over Ru/TiO2Catalysts. *ACS Catal* **2021**, *11*, 8104–8115. https://doi.org/10.1021/acscatal.1c00874.

(10) Serrano, D. P.; Aguado, J.; Escola, J. M. Developing Advanced Catalysts for the Conversion of Polyolefinic Waste Plastics into Fuels and Chemicals. *ACS Catalysis*. September 7, 2012, pp 1924–1941. https://doi.org/10.1021/cs3003403.

(11) Ellen MacArthur Foundation. *The New Plastics Economy: Catalysing Action*; 2017.

(12) Morris, B. A. *The Science and Technology of Flexible Packaging: Multilayer Films from Resin and Process to End Use*; Ebnesajjad, S., Ed.; William Andrew, 2017.

(13) Butler, T. I.; Morris, B. A. *Multilayer Flexible Packaging*; Wagner Jr, J. R., Ed.; William Andrew, 2016.

(14) Henderson, A. M. Ethylene-Vinyl Acetate (EVA) Copolymers: A General Review. *IEEE Electrical Insulation Magazine* **1933**, *9* (1), 30-38. https://doi.org/10.1109/57.249923

(15) Ellis, L. D.; Rorrer, N. A.; Sullivan, K. P.; Otto, M.; McGeehan, J. E.; Román-Leshkov, Y.; Wierckx, N.; Beckham, G. T. Chemical and Biological Catalysis for Plastics Recycling and Upcycling. *Nature Catalysis*. Nature Research July 1, 2021, pp 539–556. https://doi.org/10.1038/s41929-021-00648-4.

(16) Zhang, Y.; Kang, S.; Allen, S.; Allen, D.; Gao, T.; Sillanpää, M. Atmospheric Microplastics: A Review on Current Status and Perspectives. *Earth-Science Reviews*. Elsevier B.V. April 1, 2020. https://doi.org/10.1016/j.earscirev.2020.103118.

(17) Lange, K.; Furén, R.; Österlund, H.; Winston, R.; Tirpak, R. A.; Nordqvist, K.; Smith, J.; Dorsey, J.; Viklander, M.; Blecken, G. T. Abundance, Distribution, and Composition of Microplastics in the Filter Media of Nine Aged Stormwater Bioretention Systems. *Chemosphere* **2023**, *320*. https://doi.org/10.1016/j.chemosphere.2023.138103.

(18) Wang, C.; Xie, T.; Kots, P. A.; Vance, B. C.; Yu, K.; Kumar, P.; Fu, J.; Liu, S.; Tsilomelekis, G.; Stach, E. A.; Zheng, W.; Vlachos, D. G. Polyethylene Hydrogenolysis at Mild Conditions over Ruthenium on Tungstated Zirconia. *JACS Au* **2021**, *1* (9), 1422–1434. https://doi.org/10.1021/jacsau.1c00200.

(19) Tamura, M.; Miyaoka, S.; Nakaji, Y.; Tanji, M.; Kumagai, S.; Nakagawa, Y.; Yoshioka, T.; Tomishige, K. Structure-Activity Relationship in Hydrogenolysis of Polyolefins over Ru/Support Catalysts. *Appl Catal B* **2022**, *318*. https://doi.org/10.1016/j.apcatb.2022.121870.

(20) Sultan, B.; Sörvik, E. Thermal Degradation of EVA and EBA—A Comparison. II. Changes in Unsaturation and Side Group Structure. *J Appl Polym Sci* **1991**, *43* (9), 1747–1759. https://doi.org/10.1002/app.1991.070430918.

(21) Anders, H.; Zimmermann, H. A Comparison of the Thermal Degradation Behaviours of Poly(Vinyl Acetate), Poly(Vinyl Alcohol) and Poly(Vinyl Chloride). *Polym Degrad Stab* **1987**, *18*, 122. https://doi.org/10.1016/0141-3910(87)90024-3

(22) Munteanu, D.; Turcu, S. Evaluation of Kinetic Parameters of the Thermal Decomposition of Polyethylene-Vinyl Acetate Graft Copolymers. *Journal of Thermal Analysis* **1981**, *20*, 281–289. https://doi.org/10.1007/BF01912876

(23) Sultan, B.-Å.; Sorvik, E. Thermal Degradation of EVA and EBA-A Comparison. III. Molecular Weight Changes. *J Appl Polym Sci* **1991**, *43*, 1761–1771. https://doi.org/10.1002/app.1991.070430919

(24) Kruse, M.; Wagner, M. H. Time-Resolved Rheometry of Poly(Ethylene Terephthalate) during Thermal and Thermo-Oxidative Degradation. *Rheol Acta* **2016**, *55* (10), 789–800. https://doi.org/10.1007/s00397-016-0955-2.

(25) Venoor, V.; Ratto, J. A.; Kazmer, D. O.; Sobkowicz, M. J. Analysis of Post-Condensation and Thermo-Oxidative Degradation in Cycloaliphatic Polyamide through Time-Resolved Rheology (TRR). *Rheol Acta* **2022**, *61* (4–5), 319–337. https://doi.org/10.1007/s00397-022-01327-2.

(26) Makrodimitri, Z. A.; Heller, A.; Koller, T. M.; Rausch, M. H.; Fleys, M. S. H.; Bos, A. N. R.; Van Der Laan, G. P.; Fröba, A. P.; Economou, I. G. Viscosity of Heavy N-Alkanes and Diffusion of Gases Therein Based on Molecular Dynamics Simulations and Empirical

Correlations. *Journal of Chemical Thermodynamics* **2015**, *91*, 101–107. https://doi.org/10.1016/j.jct.2015.07.026.

(27) Winter, H. H.; Chambon, F. Analysis of Linear Viscoelasticity of a Crosslinking Polymer at the Gel Point. *J Rheol (N Y N Y)* **1986**, *30* (2), 367–382. https://doi.org/10.1122/1.549853.

(28) Hendra, P. J.; Agbenyega, J. K. (Jonathan K.). *The Raman Spectra of Polymers / P.J. Hendra and J.K. Agbenyega*; Chichester ; New York : John Wiley & Sons, c1993, 1993.

(29) Olcay, H.; Xu, Y.; Huber, G. W. Effects of Hydrogen and Water on the Activity and Selectivity of Acetic Acid Hydrogenation on Ruthenium. *Green Chemistry* **2014**, *16* (2), 911–924. https://doi.org/10.1039/c4gc00011k.

(30) Olcay, H.; Xu, L.; Xu, Y.; Huber, G. W. Aqueous-Phase Hydrogenation of Acetic Acid over Transition Metal Catalysts. *ChemCatChem* **2010**, *2* (11), 1420–1424. https://doi.org/10.1002/cctc.201000134.

(31) Rimez, B.; Rahier, H.; Van Assche, G.; Artoos, T.; Biesemans, M.; Van Mele, B. The Thermal Degradation of Poly(Vinyl Acetate) and Poly(Ethylene-Co-Vinyl Acetate), Part I: Experimental Study of the Degradation Mechanism. *Polym Degrad Stab* **2008**, *93* (4), 800–810. https://doi.org/10.1016/j.polymdegradstab.2008.01.010.

(32) Wright, W. R. H.; Palkovits, R. Development of Heterogeneous Catalysts for the Conversion of Levulinic Acid to γ-Valerolactone. *ChemSusChem* **2012**, *5* (9), 1657–1667. https://doi.org/10.1002/cssc.201200111.

(33) Sichina, W. J. *DSC as Problem Solving Tool: Measurement of Percent Crystallinity of Thermoplastics*; 2000. www.perkinelmer.com. (accessed September 12th, 2023)

(34) Ferrari, A. C.; Robertson, J. Interpretation of Raman Spectra of Disordered and Amorphous Carbon. *Phys Rev B* **2000**, *61* (20), 14095.

(35) Zhang, H.; Shao, S.; Xiao, R.; Shen, D.; Zeng, J. Characterization of Coke Deposition in the Catalytic Fast Pyrolysis of Biomass Derivates. In *Energy and Fuels*; 2014; Vol. 28, pp 52–57. https://doi.org/10.1021/ef401458y.

(36) Serrano, D. P.; Aguado, J.; Escola, J. M.; Rodríguez, J. M.; Morselli, L.; Orsi, R. Thermal and Catalytic Cracking of a LDPE-EVA Copolymer Mixture. In *Journal of Analytical and Applied Pyrolysis*; Elsevier, 2003; Vol. 68–69, pp 481–494. https://doi.org/10.1016/S0165-2370(03)00037-8.

(37) Lu, J.; Faheem, M.; Behtash, S.; Heyden, A. Theoretical Investigation of the Decarboxylation and Decarbonylation Mechanism of Propanoic Acid over a Ru(0 0 0 1) Model Surface. *J Catal* **2015**, *324*, 14–24. https://doi.org/10.1016/j.jcat.2015.01.005.

(38) Ibrahim, B.; Katritzky, A. R.; Smith, A.; Weiss, D. E. Carbon-13 Nuclear Magnetic Resonance Spectroscopy of Polymers. Part I. High Resolution Carbon-13 Nuclear Magnetic Resonance Spectroscopy: Tacticity Studies on Poly(Vinyl Acetate) and Monomer Distribution Analysis in Ethylene-Vinyl Acetate Copolymers. *Journal of the Chemical Society, Perkin Transactions 2* **1974**, No. 13, 1537–1542. https://doi.org/10.1039/p29740001537.

(39) Kuwahara, R.; Tomita, R.; Ogawa, N.; Nakajima, K.; Takeda, T.; Uehara, H.; Yamanobe, T. Crystallization and Hardening of Poly(Ethylene-Co-Vinyl Acetate) Mouthguards during Routine Use. *Sci Rep* **2017**, *7*. https://doi.org/10.1038/srep44672.

(40) Mcgrath, M. P.; Sail, E. D.; Tremont, S. J. Functionalization of Polymers by Metal-Mediated Processes. *Chem. Rev* **1995**, *95*, 381–398. https://doi.org/10.1021/cr00034a004

(41) Vance, B. C.; Kots, P. A.; Wang, C.; Hinton, Z. R.; Quinn, C. M.; Epps, T. H.; Korley, L. S. T. J.; Vlachos, D. G. Single Pot Catalyst Strategy to Branched Products via Adhesive Isomerization and Hydrocracking of Polyethylene over Platinum Tungstated Zirconia. *Appl Catal B* **2021**, *299*. https://doi.org/10.1016/j.apcatb.2021.120483.

(42) Wells, P. B., The Platinum Metals as Selective Hydrogenation Catalysts. *Platinum Metals Review* **1963**, 7 (1), 18-24. https://doi.org/10.1595/003214063X711824

(43) Speight, J. G. *Handbook of Petrochemical Processes*. https://www.crcpress.com/Chemical-Industries/. (accessed September 12th, 2023)

(44) Tamura, M.; Shimizu, K. I.; Satsuma, A. Comprehensive IR Study on Acid/Base Properties of Metal Oxides. *Appl Catal A Gen* **2012**, *433–434*, 135–145. https://doi.org/10.1016/j.apcata.2012.05.008.

(45) Shimadzu. *Application Note Quantitation of Vinyl Acetate in EVA-FTIR*. www.shimadzu.de. (accessed September 12th, 2023)

(46) Hinton, Z. R.; Kots, P. A.; Soukaseum, M.; Vance, B. C.; Vlachos, D. G.; Epps, T. H.; Korley, L. T. J. Antioxidant-Induced Transformations of a Metal-Acid Hydrocracking Catalyst in the Deconstruction of Polyethylene Waste. *Green Chemistry* **2022**, *24* (19), 7332–7339. https://doi.org/10.1039/d2gc02503e.

Graphical Abstract

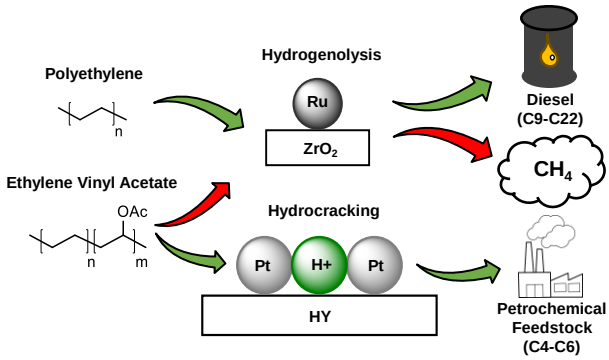

Synopsis

Ethylene vinyl acetate plastic waste can be reintroduced into the carbon economy as a useful petrochemical feedstock instead of producing methane.